

1 Interfacial supercooling and the precipitation of hydrohalite in frozen 2 NaCl solutions by X-ray absorption spectroscopy

3 Thorsten Bartels-Rausch¹, Xiangrui Kong^{1*}, Fabrizio Orlando^{1**}, Luca Artiglia¹, Astrid Waldner¹,
4 Thomas Huthwelker², Markus Ammann¹

5 ¹Laboratory of Environmental Chemistry, Paul Scherrer Institut, Villigen PSI, Switzerland

6 ²Swiss Light Source (SLS), Paul Scherrer Institut, Villigen PSI, Switzerland

7 * now at: Department of Chemistry and Molecular Biology, Atmospheric Science, University of Gothenburg, Gothenburg,
8 Sweden

9 ** now at: Omya International AG, Oftringen, Switzerland

10
11
12
13 *Correspondence to:* Thorsten Bartels-Rausch (thorsten.bartels-rausch@psi.ch)

14 **Abstract.** Laboratory experiments are presented on the phase change at the surface of sodium chloride – water mixtures at
15 temperatures between 259 K and 240 K. High selectivity to the upper few nanometres of the frozen solution – air interface is
16 achieved by using electron yield near-edge X-ray absorption fine structure (NEXAFS) spectroscopy. We find that sodium
17 chloride at the interface of frozen solutions, which mimic sea-salt deposits in snow, remain as supercooled liquid down to
18 240 K. Once efflorescence occurred, hydrohalite formed, for which we present the NEXAFS spectrum. At the interface,
19 hydrohalite exclusively precipitates, anhydrous sodium chloride is not detected. The hydrohalite is found to be stable while
20 increasing the temperature towards the eutectic temperature of 253 K. Taken together, this study reveals no differences in the
21 phase changes of sodium chloride at the interface as compared to the bulk. That sodium chloride remains liquid at the interface
22 upon cooling down to 240 K, which spans the most common temperature range in Polar marine environments, has
23 consequences for interfacial chemistry involving chlorine as well as for any other reactant for which the sodium chloride
24 provides a liquid reservoir at the interface of environmental snow.

25 1 Introduction

26 Chemical cycling of halogens affects the composition of the troposphere and via this effect influences climate and impacts
27 human health (Simpson et al., 2007; Abbatt et al., 2012; Saiz-Lopez and von Glasow, 2012; Simpson et al., 2015). Taken the
28 abundance of chloride in the form of sea-salt over wide areas of the globe, the atmospheric chemistry of chlorine has long
29 raised interest in a number of multiphase reactions that liberate chloride into chlorine species in the gas phase. Chlorine has a
30 direct role as a sink for ozone. Further, reactive chlorine species act as a powerful oxidant on atmospheric cycles that destroy
31 or produce ozone and are relevant for the atmospheric oxidation capacity (Finlayson-Pitts, 2003; Thornton et al., 2010).
32 Atmospheric ozone is of concern because it directly impacts atmospheric composition, health, and climate (Simpson et al.,

33 2007). A prominent example of these reactions with chloride in sea-salt or salt-dust are acid displacements, where the nitric or
34 sulfuric acid are taken up into the aqueous phase, and subsequently hydrochloric acid is emitted to the gas phase. Further
35 examples are reactions with OH radicals (Knipping et al., 2000), and with nitrogen oxides (Osthoff et al., 2008). Common to
36 all of these reactions is the generation of chlorine gases that either react with OH radicals or photolyze at wavelengths available
37 in the troposphere to generate reactive chlorine. Given their importance, these multiphase reactions have intensively been
38 investigated in laboratory studies over the last decade (Abbatt et al., 2012; Saiz-Lopez and von Glasow, 2012; Simpson et al.,
39 2015). One outcome of these investigations is the importance of reactions at the liquid – air interface as compared to those
40 proceeding in the bulk. An example is the oxidation of chloride by OH radicals. In contrast to the aqueous phase reactions, it
41 does not require the presence of acid to proceed fast at the air—water interface (Laskin et al., 2006).

42
43 The relevance of halogen multiphase chemistry is not limited to chlorine. A more recent example is the oxidation of bromide
44 to hypobromous acid. Bromide is present in sea-salt, is a key reactant in polar ozone depletion by itself (Simpson et al., 2015),
45 and participates in chlorine chemistry by forming interhalogen compounds (Finlayson-Pitts, 2003). Oldridge and Abbatt (2011)
46 have shown that a Langmuir-Hinshelwood type surface reaction of ozone with bromide occurs at the liquid – air interface
47 simultaneously with a corresponding bulk reaction in the temperature range of 263 K to 248 K. A surface-active reaction
48 intermediate was found to explain the high interfacial reactivity for the case of the reaction with ozone (Artiglia et al., 2017),
49 while other bromine species may directly exhibit surface propensity on their own (Gladich et al., 2020). Clearly, this line of
50 research shows how reaction kinetics and mechanisms differ at the interface from those in the bulk and that heterogeneous
51 chemistry is a key driver in atmospheric chemistry.

52
53 It is further known that reactivity critically depends on the phase and liquid content of the reaction medium (Bartels-Rausch
54 et al., 2014; Kahan et al., 2014). Importantly, it is not only the chlorine chemistry that responds to the phase of sodium chloride
55 present. Oldridge and Abbatt (2011) showed that the rate of the heterogeneous reaction of ozone with bromide in sodium
56 chloride -- water mixtures is strongly reduced once sodium chloride precipitates below 252 K and consequently the liquid
57 volume in the sample is reduced. Similar, the photolytical reaction of nitroanisol with pyridine was found to depend on the
58 amount of liquid in frozen samples and thus to critically respond to precipitation of sodium chloride (Grannas et al., 2007).
59 Next to its role in atmospheric halogen chemistry, sodium chloride is thus further of importance as salt to establish and maintain
60 liquid solutions at subfreezing temperature. Its importance arises from its atmospheric abundance but also because its eutectic
61 temperature of 252 K falls into typical springtime Arctic temperatures – a region and time period when atmospheric halogen
62 chemistry is most active.

63
64 While the phase diagram of sodium chloride – water binary mixtures and the thermodynamic stability domains of salt, solution,
65 and ice are well known (Koop et al., 2000), the precise occurrence of nucleation and sodium chloride precipitation is still
66 debated (Koop et al., 2000; Wise et al., 2012; Peckhaus et al., 2016). Koop et al. (2000) were the first to show that because

67 precipitation of sodium chloride can be kinetically hindered, supercooled sodium chloride solutions in presence of ice can
68 prevail down to 240 K. Cho et al. (2002) has observed a liquid fraction in sodium chloride – water mixtures between 228 K
69 and 273 K based on the evaluation of $^1\text{H-NMR}$ signals. Cho et al. (2002) proposed the presence of liquid below the eutectic
70 temperature to be an interfacial phenomenon, stabilized by surface forces in analogy to the disordered interface observed for
71 neat ice surfaces when approaching the melting point (Bartels-Rausch et al., 2014).

72
73 The appearance of hydrohalite at air-ice interfaces is also of interest to sea ice research, because precipitation of hydrohalite
74 increases the albedo of sea ice. During the Snowball Earth period, 700 million years before present, climatic conditions may
75 have favoured the existence of hydrohalite with its climatic feedback (Light et al., 2009). For modern Earth, precipitation of
76 brine constituents in sea ice is relevant for ion mobility and might result in ion fractionation during wash out events (Maus et
77 al., 2008; Obbard et al., 2009; Maus et al., 2011). Precipitation of sodium chloride in sea spray aerosol in the troposphere, not
78 embedded in snow or sea ice, is further of ongoing interest. The focus is placed on whether anhydrous sodium chloride (halite)
79 or hydrohalite precipitates. In regions of the phase diagram, where the hydrohalite is the thermodynamic stable form,
80 precipitation of the halite was observed with impacts on stability of the solid phase upon warming and or humidification, since
81 the deliquesce relative humidity of the two compounds differs by 6 percentage points (Wagner et al., 2012; Wise et al., 2012;
82 Peckhaus et al., 2016).

83
84
85 The goal of this study is to investigate the precipitation and the occurrence of liquid features in sodium chloride – water binary
86 mixtures in the interfacial region. Both Cho et al. (2002) and Koop et al. (2000) have applied methods that are not specifically
87 sensitive to the interface, but are probing the bulk. Near Edge X-ray Absorption Fine Structure (NEXAFS) spectroscopy is
88 inherently sensitive to the upper few nanometer of interfaces when detecting electrons as done in this work. Oxygen K-edge
89 NEXAFS spectra of H_2O are an established tool to investigate the hydrogen bonding structure of water and ice (Bluhm et al.,
90 2002; Nilsson et al., 2010; Krepelova et al., 2013; Newberg and Bluhm, 2015; Orlando et al., 2016; Bartels-Rausch et al.,
91 2017; Ammann et al., 2018; Waldner et al., 2018). In our earlier NEXAFS study (Krepelova et al., 2010a), it was shown by
92 probing the X-ray absorption of oxygen atoms in sodium chloride – water binary mixtures that the hydrogen bonding network
93 did not reveal the presence of any liquid features at the interface below the eutectic temperature. Interpretation of these oxygen
94 NEXAFS spectra was complicated by the appearance of crystal water in the solid form of sodium chloride (hydrohalite,
95 $\text{NaCl}\cdot 2\text{H}_2\text{O}$) and by the presence of adsorbed H_2O on NaCl . Also, the oxygen spectra might be dominated by ice that is present
96 in equilibrium with the sodium chloride solution and thus small fractions of liquid might have been difficult to detect. In this
97 work, we therefore discuss Cl K-edge NEXAFS that have previously been used to inspect the chemical speciation of chlorine
98 in glasses and in coal (Huggins and Huffman, 1995; Evans et al., 2008). Interest in the local environment of chloride at the
99 interface in sodium chloride – water binary mixtures comes also from earlier work on nitric and hydrochloric acid adsorbed at
00 the ice-air interface. We have shown that nitrate and chloride forms solvation shells with a hydrogen-bonding structure similar

01 to that in aqueous solution in the interfacial region of ice at concentrations low enough to prevent melting (Krepelova et al.,
02 2010b; Kong et al., 2017). The aim of this study is thus also to investigate the occurrence of solvated chloride at the interface
03 of sodium chloride – water mixtures at temperatures close to the eutectic. Motivation comes from the role of heterogeneous
04 chemistry in atmospheric science in general and in particular on the impact that the microchemical environment has on the
05 reactivity.

06 **1 Experimental Part**

07 Experiments were performed at the PHOENIX beam line of the Swiss Light Source (SLS) at the Paul Scherrer Institute using
08 the Near Ambient Pressure Photoemission (NAPP) set-up previously described (Orlando et al., 2016). NAPP is equipped with
09 a differentially-pumped electron analyser (Scienta R4000 HiPP-2). The central feature of NAPP is a flow-through cell with a
10 sample holder the temperature of which is computer-controlled by a flow of cooled helium gas. The measurements were
11 performed with partial pressures of water between 0.3 mbar and 1.8 mbar in the flow-through cell and temperatures of the
12 sample between 259 K and 240 K.

13 **1.1 Sample Preparation and Water Dosing**

14 To prepare a sample, 1 μl of a 2.12 g sodium chloride (Fluka Trace Select 38979-25G-F) solution in 80 ml of water (Fluka
15 Trace Select 142100-12-F) was dropped at the centre of the sample holder and dried at 60 °C. The sample holder was then
16 moved into the flow-through cell and kept at UHV and at 60 °C to 80 °C for 45 minutes to remove volatile impurities. Water
17 vapour was dosed to the flow-through cell via a 0.8 mm i.d. steel capillary from the vapour above liquid water (Fluka Trace
18 Select 142100-12-F) in a vacuum-sealed, temperature-controlled glass reservoir. Before dosing, the water was degassed by 4
19 freeze-pump-thaw cycles. Pressure in the flow-through cell was monitored by a capacitance manometer (Baratron 626A) with
20 a measurement range from 5×10^{-4} to 10 mbar and an accuracy of 0.25 % of the reading. Temperature was monitored with a
21 Pt-1000 sensor located at the edge of the sample holder. The sensor was calibrated prior to the experiments by growing ice on
22 the sample holder and noting its vapour pressure which is a direct measure of the temperature at the sample spot (Marti and
23 Mauersberger, 1993). During the experiments, the calibration was confirmed when ice was present. At 253 K, the offset
24 between temperature reading and calibration was found to be 4.3 ± 0.2 K.

25 **1.1 X-ray excited Electron Spectroscopy**

26 Partial Auger-Meitner electron-yield NEXAFS spectra at the Cl K-edge were acquired with a fixed kinetic energy window of
27 2370 eV to 2390 eV, which includes the KL_{2,3}L_{2,3} Auger-Meitner peak of chlorine. The pass energy and dwell time were set
28 to 200 eV and 300 ms, respectively. The distance of the sample to the electron analyser inlet (working distance) was 1 mm
29 and the electron analyser was operated with an electron sampling aperture with a diameter of 500 μm . NEXAFS spectra were
30 measured by sweeping the incident X-ray photon energy across the chlorine K-edge from 2815 eV to 2845 eV with steps

31 ranging from 0.2 eV to 1 eV. The NEXAFS spectra were processed by dividing by the photon flux (I_0) as derived *in-situ* using
32 a Ni coated membrane, by subtracting the mean pre-edge intensity as background, and by normalising to the mean intensity at
33 2830 eV to 2833 eV X-ray photon energy. Photoemission spectra (XPS) of O1s, Cl2p, Na1s, C1s, and Au4f were recorded at
34 an incident X-ray photon energy of 2200 eV and a with a pass energy of 100 eV and a dwell time of 120 ms. To quantify, a
35 linear background was applied and the photoemission signal was integrated in Matlab without any peak fitting.

36 **1 Results and Discussion**

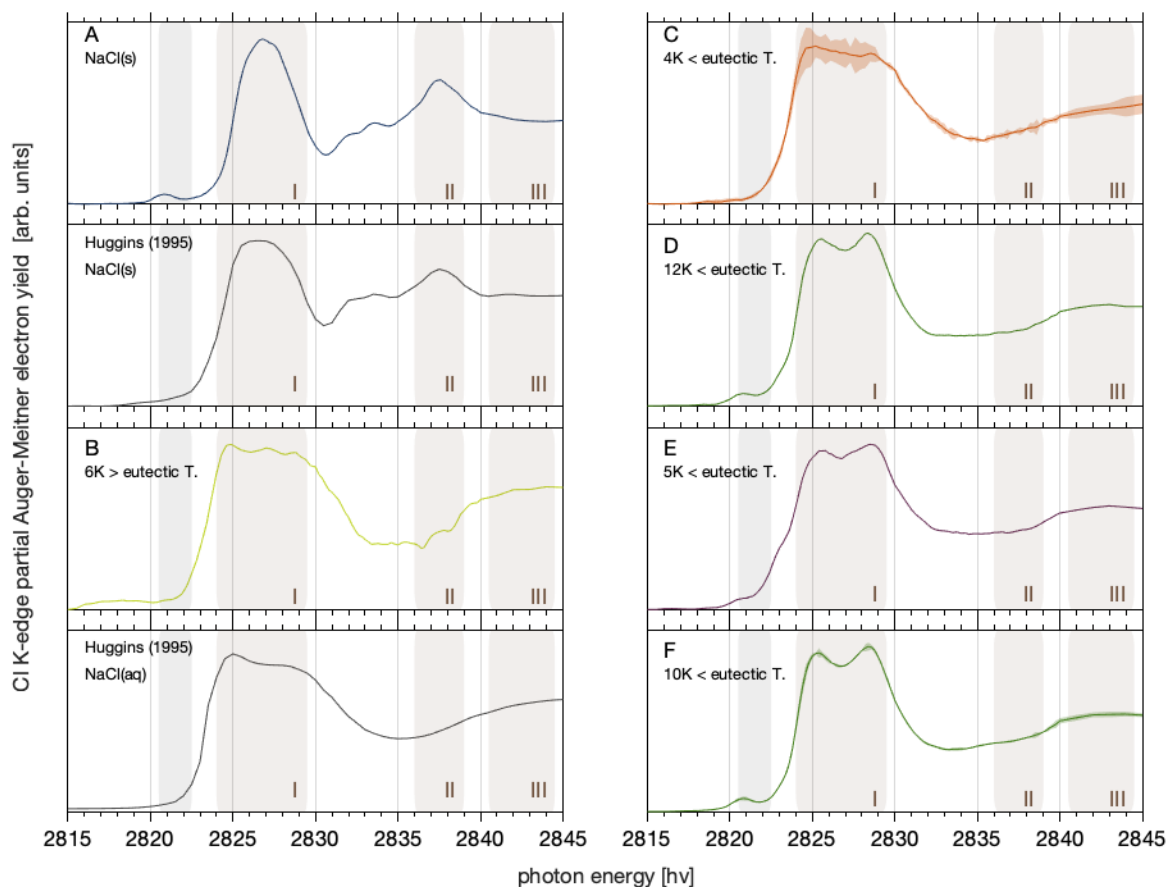
37 **NEXAFS of brine, halite, and hydrohalite**

38 Figure 1 shows chlorine K-edge X-ray absorption spectra of solid NaCl and of frozen NaCl-water binary mixtures in presence
39 of ice. NEXAFS spectroscopy probes the X-ray absorption of chlorine atoms, that is the resonant excitation of core electrons
40 into unoccupied molecular orbitals. As exactly those outer orbitals are forming chemical bonds, NEXAFS spectra directly
41 reflect changes to the local chemical environment and structural arrangement. NEXAFS spectroscopy of halogen salts has thus
42 been used to discuss their phase and chemical speciation in geological examples (Huggins and Huffman, 1995; Evans et al.,
43 2008). In this work, the X-ray absorption spectra were derived by recording the intensity of Auger-Meitner electrons at 2370-
44 2390 eV, which corresponds to the KL_{2,3}L_{2,3} transition in chlorine (Cleff and Mehlhorn, 1969). Detecting electrons, as done
45 in this work, makes X-ray absorption inherently surface sensitive, because electrons have a limited escape depth in matter
46 (Ammann et al., 2018). The escape depth can be quantified by relating it to the inelastic mean free path (IMFP) of electrons in
47 matter and to the take-off angle of detected relative to the surface normal. The IMFP of electrons with a kinetic energy of
48 2380 eV is about 7 nm in NaCl and in ice (Tanuma et al., 1991). The take-off angle of electron detection is 30° in our set-up
49 (Orlando et al., 2016), this gives an escape depth of 6 nm, meaning that cumulatively, 95% of the electrons detected originate
50 from 18 nm, with an exponentially decreasing contribution from the surface towards the bulk. In the following, we report the
51 NEXAFS spectra derived from this interfacial region of NaCl-water binary mixtures to discuss changes in the solvation of
52 chloride by water as we explore the regions of the phase diagram where precipitation and efflorescence of sodium chloride has
53 been described for bulk samples.

54
55 All chlorine K-edge spectra show a strong absorption peak at 2825-2830 eV (region I), the absorption edge, corresponding to
56 the transition of electrons from the 1s to the empty 4p orbitals. Solid NaCl salt, in Fig. 1 A, shows a strong absorption in
57 region I, and a characteristic feature at 2838 eV (region II) (Huggins and Huffman, 1995; Evans et al., 2008). The difference
58 in the relative intensity of region I as compared to the intensity at photon energies > 2830 eV between Fig. 1A and Huggins
59 and Huffmann (1995) comes from the latter using fluorescence as detection mode. Detecting X-ray absorption with
60 fluorescence probes deeper into the bulk of the samples and therefore often suffers from self-absorption which leads to less
61 signal intensities at the absorption edge (region I).

62

63 The small feature at 2821 eV can be assigned to C-Cl bonds that may form in-situ due to reactions involving secondary
64 electrons and organic impurities (Fujimori et al., 2010). The sample composition in the interfacial region was further
65 investigated by X-ray photoemission spectroscopy. The C1s and Cl2p spectra support the presence of C-Cl compounds in the
66 samples (Supporting Info): A small feature in the Cl2p spectra at 3 eV higher binding energy than the main chlorine signal
67 might be attributed to organic carbon species. The C1s photoemission spectra show a feature at 1.5 eV higher binding energy
68 than the main feature, typical for C-Cl compounds. The main feature of the C1s photoemission spectra is attributed to C-H
69 bonds, the dominant component of adventitious carbon that forms in a cascade of reactions with secondary electrons during
70 the experiments. A further source of carbon might be omnipresent traces of carbon in the NaCl and introduced when preparing
71 the NaCl samples. The atomic ratio of the total carbon to oxygen from water present at the interface was below 0.25, except
72 for samples in Fig. 1A and F where total carbon to oxygen atomic ratios were 0.5-0.75. Adsorbed water molecules were present
73 at the interface of all samples, and ice or liquid water formed in some samples, as gaseous water was present in all experiments
74 with pressures between 0.3 mbar to 1.8 mbar. The atomic ratio was derived based on the measured C1s/O1s photoemission
75 intensities and a calibration to account for the analyser efficiency and total X-ray photoionization cross section using C1s/O1s
76 photoemission intensities of 0.8 mbar CO₂ gas following a procedure used before (Krepelova et al., 2013). Direct comparison
77 between the individual samples and estimation of surface coverages of the carbon impurities is hampered by the varying water
78 content at the sample's interface as adsorption and water uptake varies with the individual relative humidity settings.
79



81

82 **Figure 1:** Partial electron yield chlorine K-edge NEXAFS spectra of the sodium chloride -- water binary system: Solid NaCl at 248 K and
 83 44 % relative humidity (A), aqueous NaCl solution in equilibrium with ice at 88 % RH and 259 K (B), an averaged spectrum at the
 84 thermodynamic ice stability line at 248-249 K (C), an individual spectrum upon further cooling to 240 K (D), and upon heating back to
 85 249 K in the ice stability domain (E). Fig. 1F shows the averaged spectrum at 244 K and relative humidities of 59 % and 73 %, lower than
 86 the ice stability domain. See Fig. 2 for precise measurement settings. The shaded area in the colour of the graph in C and F denote the
 87 standard deviation of 3 and 2 repeated NEXAFS acquisitions. Also shown are NEXAFS spectra of NaCl salt and aqueous solutions for
 88 comparison that were detected in fluorescence mode and not in partial electron yield (Huggins and Huffman, 1995). The brownish shaded
 89 area (I-III) highlights regions in the NEXAFS spectra disused in the text. The grey shaded area at 2821 eV highlights the photon energy
 90 region where carbon-chlorine bonds from carbon contamination might show an absorption feature (see text for details).

91

92

93 The spectrum of sodium chloride in aqueous solution, Fig. 1B, shows a broader absorption peak in region I compared to the
94 spectra of the halite and a second feature at 2840 eV (region III) (Huggins and Huffman, 1995). In this work, the NEXAFS
95 spectrum of NaCl in aqueous solution was recorded in a solution-ice binary mixture based on the phase diagram (see
96 Efflorescence at the Interface). Based on freezing point depression data, the concentration of sodium chloride in such an
97 aqueous solution in equilibrium with ice is 3.5 mol l⁻¹ (2019). The spectrum in Fig 1B generally agrees with the X-ray
98 absorption spectra reported for 0.1 mol l⁻¹ and 1 mol l⁻¹ aqueous solutions (Fig. 1 Huggins and Huffman (1995)) as it captures
99 the general decrease in intensity in region I with excitation energy and the increase in absorption in region III (Fig. 1).
00 Discussing differences in the hydration structure of chloride at the water—air interface as compared to the bulk solution is
01 beyond the scope of this work. Harada et al. (2011) has reported differences in the hydration structure of Br⁻ at the aqueous
02 surface compared to in bulk. Due to the low spectrum quality, evident by the wiggles in region I, we refrain from discussing
03 the two distinct features in region I, at 2824 eV and 2829 eV, that have been observed in previous work on NEXAFS spectra
04 of aqueous chloride solution (Huggins and Huffman, 1995; Antalek et al., 2016).

05
06 Figure 1C-E show NEXAFS spectra acquired in the ice stability domain at temperatures below the eutectic temperature of
07 251.9 K (Koop et al., 2000). At 248-249 K, the NEXAFS spectrum resembles that of a typical aqueous solution (Figure 1C).
08 Figure 1C shows an average of 3 individual NEXAFS spectra which still shows substantial scatter that results in low spectra
09 quality. We assign this to the low amount of salt within the interfacial region and to potential thermal circulations and thus
10 redistribution of the liquid upon irradiation by the beam. Despite this uncertainty, the results in Fig. 1A-C allow to clearly
11 differentiate between solid halite and aqueous solution.

12
13 Upon cooling further to 241 K, the spectrum changed significantly. The NEXAFS spectrum in Fig. 1D shows a wide peak in
14 region I with two well resolved features about 3 eV apart. That both features have a similar intensity, makes this spectrum
15 clearly distinct from those of an aqueous NaCl solution with its decreasing trend of absorption in region I. Compared to the
16 spectrum of aqueous NaCl solution (Fig. 1B, C), the absorption edge is shifted to higher photon energies in the spectrum in
17 Fig. 1D. The absence of a feature in region II makes the spectrum in Fig. 1D distinct them from the spectrum of anhydrous
18 NaCl salt. Notably, the spectrum quality is greatly improved and is similar to that of the solid anhydrous NaCl sample (Fig.
19 1A). One factor impacting the spectral quality is the stability of the sample during the NEXAFS acquisition. The analysis of
20 the Cl 2p photoemission spectra acquired before and after each NEXAFS run showed that the amount of chlorine detected in
21 the sample volume fluctuated by less than 10%, between 0 % and 9 %, in samples shown in Fig. 1 C, D, E, and F (Supporting
22 Information). For comparison, samples in Fig. 1 A and B showed a decrease of 39 % and 43 % in the integrated Cl 2p signal
23 intensity, respectively, from prior- to after the NEXAFS was recorded. Possible reasons for these trends are an increase in
24 adsorbed water with time masking the intensity of the underlying chlorine (Fig. 1A) and changes in the distance of the sample
25 to the electron analyser with time leading to a reduction in the intensities of all compounds (Fig. 1 B). See supporting
26 information for further discussion. Both of these processes would also affect the NEXAFS signal by inducing changes in

27 intensity with time. Direct quantitative comparison is beyond the scope of this work, and is hampered by the different probing
28 depth of XPS and NEXAFS as given by the kinetic energy.

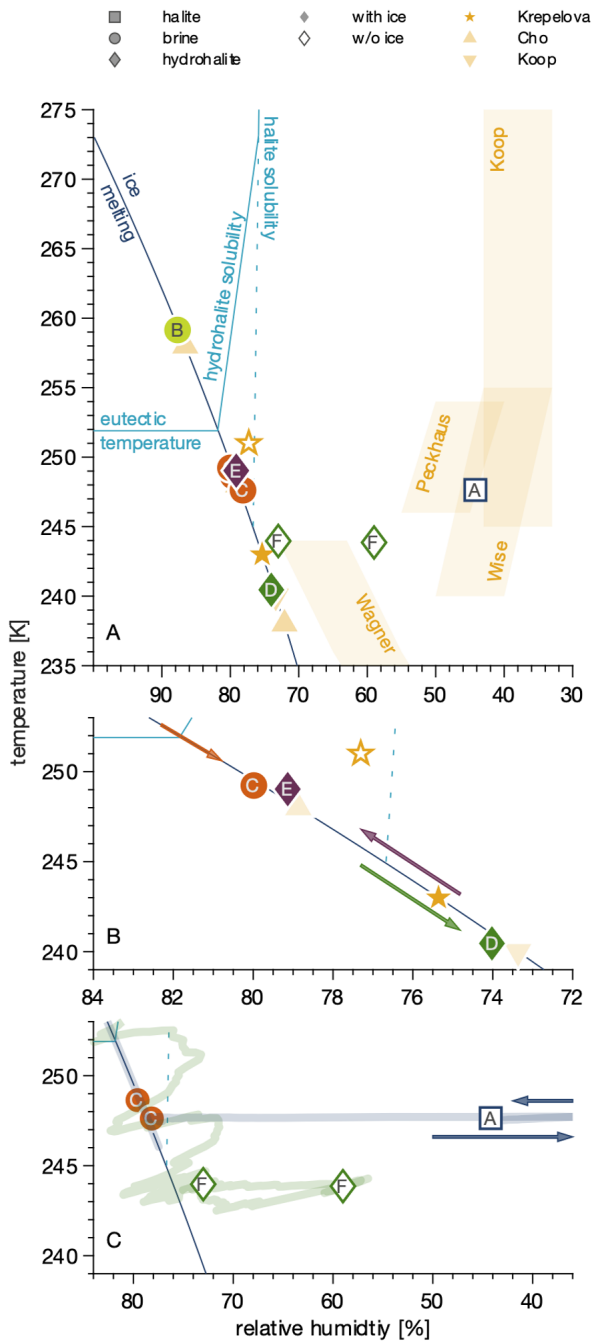
29

30 We assign the spectrum in Fig. 1D to that of sodium chloride dihydrate (hydrohalite, $\text{NaCl}\cdot 2\text{H}_2\text{O}$). The NEXAFS spectrum of
31 the hydrohalite has to the best of our knowledge not been described before. The double peak feature in region I we observe
32 here is typical for other chloride hydrates such as $\text{MnCl}_2\cdot 4\text{H}_2\text{O}$, $\text{CaCl}_2\cdot 2\text{H}_2\text{O}$, and $\text{MgCl}_2\cdot 6\text{H}_2\text{O}$ (Evans et al., 2008). It is also
33 present in the NEXAFS spectra of sodium chloride solution (Huggins and Huffman, 1995), with a different ratio of the two
34 features as observed here for the hydrohalite. Antalek et al. (2016) has explained this double peak feature in NEXAFS spectra
35 of aqueous chloride solutions by the formation of two distinct solvation shells with two distances between the chloride and the
36 solvating water molecules based on NEXAFS and extended X-ray absorption fine structure spectroscopy as well as molecular
37 dynamics simulations. We propose here that the NEXAFS spectra of the hydrohalite can be understood based on the same
38 argument, as the chloride in $\text{NaCl}\cdot 2\text{H}_2\text{O}$ is coordinated by two sodium and four water molecules with differences in the distance
39 of each Cl to the neighbouring oxygen of the water molecules (Klewe et al., 1974).

40

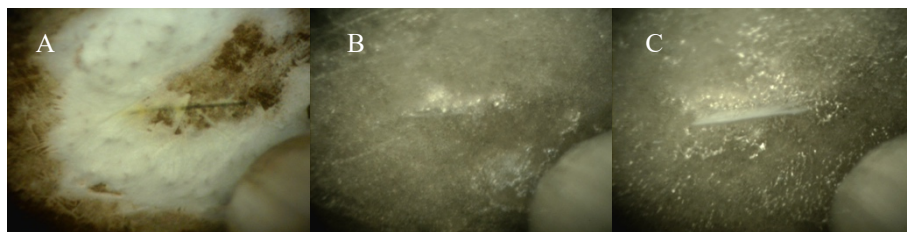
41 Figures 1E and 1F show hydrohalite spectra after warming the sample back to 249 K in presence of ice and at 244 K in absence
42 of ice. We'd like to note the excellent reproducibility of the spectra as seen in Fig. 1F by the small standard deviation of two
43 samples (shaded area). In summary, we have clearly presented three different chlorine K-edge NEXAFS spectra and argued
44 that these derive from the halite, chloride solution, and the hydrohalite. Hydrohalite at the air-ice interfacial region was thus
45 observed in the temperature range 241 K – 249 K.

46

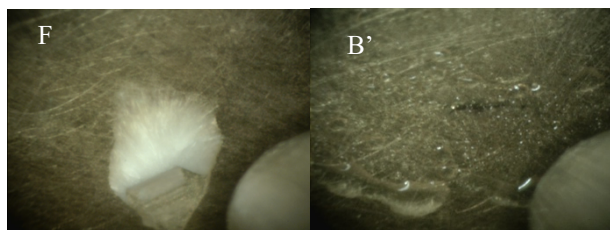


85
86
87
88

89



90
91



92
93

94 **Figure 3:** Optical microscopy pictures of the frozen samples. Each picture shows a 1 mm wide section of the sample holder with the sample.
95 The letters refer to the samples in Figs. 1 & 2. Picture B' shows the deliquesced sample prior to freezing.

96

97

98

99 **Efflorescence at the interface**

00 Now that we have identified halite, the hydrohalites, and the aqueous solution by means of the NEXAFS spectra at the
01 interfacial region, we discuss their observation in the phase diagram. Figure 2A shows the sodium chloride – water phase
02 diagram in the temperature – relative humidity space as initially constructed by Koop et al. (2000). In this work, the relative
03 humidity (RH) is referenced to the vapour pressure of (supercooled) water as parameterised by Marti and Mauersberger (1993).
04 There are two sets of experiments, those where ice is present and the sodium chloride is in equilibrium with ice (filled symbols)
05 and experiments in absence of ice (open symbols) that were done with a relative humidity less than the ice stability line in the
06 phase diagram (dark blue line). Generally, we have observed solid sodium chloride at temperatures below 240 K and at 44 %
07 to 79 % RH and brine in the temperature range of 248 K to 259 K and RH of 78 % - 88 %.

08

09 **Liquid below eutectic and nucleation**

10 In a typical experiment, anhydrous salt was exposed to increased relative humidity at a fixed temperature of 259 K. The relative
11 humidity was increased by increasing the flux of water vapour into the experimental cell. Once the relative humidity reached
12 72 %, the sample started to dissolve by water up-take from the gas-phase and an aqueous solution was formed (brine). This
13 phase change was evident by the sample becoming shiny and then forming transparent spheres as observed by an endoscope
14 digital camera (Fig. 3B'). Then, the relative humidity was further increased and/or temperature was lowered to cross the ice
15 stability line until ice nucleation occurred at a modest oversaturation. Ice nucleation was evident by a sharp pressure drop from
16 the pressure dosed to the cell to the water vapor pressure of ice at that temperature. Generally, in presence of ice, the partial
17 pressure of water in the flow-through cell is given by the vapor pressure of ice and thus a sole function of temperature. If the
18 water vapour pressure upstream of the flow through cell exceeds this value, the ice on the sample holder is growing, if it is set
19 below, the ice evaporates. Based on the calibration of the dosing reservoir temperature and partial pressure of water in the
20 flow-through cell (in absence of ice), the incoming H₂O vapour flux was adjusted such that the equilibrium pressure in the cell
21 matched the vapour pressure of ice.

22

23 A NEXAFS spectrum was acquired at 259 K and 1.82 mbar on the ice stability line and taken as reference for aqueous sodium
24 chloride solution (Fig 1B). When the temperature was lowered while adapting the flux of water into the set-up to match the
25 vapour pressure of ice at 248 K - 249 K, thus 4 K to 5 K below the eutectic temperature (Fig. 2B), the NEXAFS spectra
26 revealed that the chloride at the air-ice interface is in an environment identical to aqueous chloride (Fig. 1C). While cooling
27 further and adjusting the vapor pressure to match that of ice at each temperature, a sudden change in the sample appearance,
28 becoming less transparent, was observed by the digital endoscope, indicating efflorescence of the sample. A NEXAFS
29 spectrum recorded reveals that hydrohalite has precipitated from the brine at 240.5 K and 74 % RH (Fig. 1D). Krepelova et al.
30 (2010a) has studied phase changes of sodium chloride at the interfacial region of sodium chloride – water binary mixtures

31 previously. They have probed the oxygen with XPS and partial electron yield NEXAFS spectroscopy and concluded that, in
32 presence of ice, hydrate forms about 11 K below the eutectic (filled star in Fig. 2). Consistent with that, the chloride has a local
33 environment indistinguishable from that of the hydrate 11.4 K below the eutectic temperature and in presence of ice in the
34 current study. Our results of precipitation in presence of ice surfaces agree with the crystallization temperature observed by
35 Koop et al. (2000). We lack a direct comparison to the bulk, because the electron yield NEXAFS spectroscopy used in our
36 work is inherently surface sensitive. Cooling sodium chloride solutions of varying concentration, Koop et al. (2000) found
37 precipitation of hydrohalite at 240 K in presence of ice for bulk samples. Because precipitation occurred at 20 K higher
38 temperatures compared to emulsion samples of the same concentration, the authors concluded that the presence of surfaces
39 enhance the crystallization rate. In that study, the hydrohalite was identified by the melting temperatures of the ice-hydrohalite
40 mixtures. Malley et al. (2018) observed crystallization of sodium chloride solutions 1 K below the eutectic temperature in
41 presence of ice. The hydrohalite was clearly identified using bulk sensitive Raman spectroscopy. This difference in
42 crystallization temperature may reflect the stochastic character of freezing, as already noted by Koop et al. (2000) when
43 discussing the scatter in their data. The precise crystallization temperature is also influenced by freezing rate, concentration,
44 and the availability of surfaces (Bartels-Rausch et al., 2014). It appears thus that the precise occurrence of crystallisation is
45 governed by stochastics both at the surface and in heterogeneous freezing of the bulk.

46

47 To investigate whether or not the hydrohalite is the thermodynamically stable form at the interface at temperatures close to the
48 eutectic temperature, the sample at 240 K (green filled triangle, Fig. 2B) was warmed towards the eutectic temperature while
49 staying in the ice stability domain. Acquiring a NEXAFS spectrum (Fig. 1E) that resembles that of hydrohalite, shows that the
50 hydrohalite salt is the thermodynamically stable form also at temperatures close to the eutectic. We therefore interpret the
51 existence of liquid during the previous cooling of the sample (Fig. 2B, orange circle, Fig. 1C) at the interface as supercooled
52 solution. The sample was kept at this condition for 3 h and showing that liquid can exist for extended times at the air-ice
53 interface below the eutectic temperature and that the temperature alone is not sufficient to predict its presence. Rather the
54 thermal history of the snow needs to be considered.

55

56 For samples that were cooled to temperatures that triggered efflorescence, the chlorine NEXAFS spectra show that the
57 hydrohalite is the dominating, thermodynamically stable phase at the interface of frozen sodium chloride – water binary
58 mixtures. Cho et al. (2002) have shown that when frozen aqueous solutions were warmed, a liquid fraction was observed
59 below the eutectic temperatures. In their experiments, ice was frozen in NMR tubes lowering the temperature to 228 K in
60 15 min. which is significantly colder than the efflorescence temperatures observed here and by Koop et al. (2000). After 10
61 minutes, the samples were warmed and NMR signals were recorded. Interestingly, Cho et al. (2002) have observed the liquid
62 fraction only in experiments where the sodium chloride concentration in the initial aqueous solution was below 0.01 mol l^{-1} .
63 If the initial aqueous solution had a concentration of 0.5 mol l^{-1} no indication of liquid features below the eutectic were found.
64 Tasaki et al. (2010) has shown a similar concentration dependence for sodium bromide solutions using X-ray absorption

65 reporting solvated bromide in the bulk of the samples below the eutectic temperature only for concentrations below 50 mmol l⁻¹.
66 The experiments described here started with an aqueous solution that was formed in-situ and was kept in equilibrium with
67 a vapour pressure of roughly 1.9 mbar. The chloride concentration in such solutions is close to the concentration in a solution
68 at 1.8 mbar and at 259 K, where ice nucleation occurred and where the freezing point depression data give a concentration of
69 3.5 mol l⁻¹. This concentration can be directly compared to the concentration in the initial solutions of Cho et al. (2002), which
70 ranged from below 0.01 mol l⁻¹ to 0.5 mol l⁻¹. This back-of-the-envelope calculation thus suggests that the concentration of the
71 solutions from which ice nucleated in the experiments reported here exceeded those described by Cho et al. (2002) for which
72 no liquid fraction was observed.

73

74 The concentration of the initial solution from which ice precipitated, determines the ice to brine ratio. This is, because as the
75 concentration of the brine is a sole function of temperature, the volume of the brine relative to that of ice is given by the water
76 to sodium chloride ratio in the initial solution. One might speculate that with large amounts of brine relative to ice, that is
77 concentrations of initial solutions from which ice nucleates > 0.5 mol l⁻¹, patches and inclusions are larger in size than for more
78 dilute solutions. The inverse Köhler effect reduces the melting point only for inclusions in the nanometre range (Nye, 1991;
79 Aristov et al., 1997; Christenson, 2001; Bartels-Rausch et al., 2014), which might explain the absence of liquid features both
80 in the results reported here at the interface of ice and in the high concentration samples of Cho et al. (2002). Support for large
81 patches at the interface when solutions are frozen comes from microscopy studies. Low temperature scanning electron
82 microscopy work suggested the ice surface of frozen 0.05 mol l⁻¹ sodium chloride – water mixtures being covered by µm sized
83 brine features (Blackford, 2007; Blackford et al., 2007). Malley et al. (2018) used Raman microscopy of sodium chloride
84 solutions between 0.02 – 0.6 mol l⁻¹ initial concentration to identify µm sized, partially connected patches of liquid covering
85 11 % to 85 % of the ice surface at temperatures above the eutectic. Despite the impact of freezing temperature and rate -- that
86 differs among the individual studies -- on the distribution of impurities (Bartels-Rausch et al., 2014; Hullar and Anastasio,
87 2016), these results clearly show the tendency of µm sized features dominating at the air-ice interface. In presence of nano-
88 inclusions, we would also expect the deliquescence to occur at a lower temperature. This was not observed in our experiments,
89 suggesting the absence of nano-inclusions in the experiments presented here in the interfacial region.

90

91 We have recently reported chloride forming solvation shells in the interfacial region of ice upon adsorption of HCl at 253 K
92 (Kong et al., 2017). The surface concentration as derived from XPS suggested that it was done in the stability domain of ice,
93 i.e. the concentration of HCl was too low to melt the ice. Oxygen K-edge NEXAFS spectra showed that a substantial fraction
94 of the water molecules at the air-ice interface is arranged in a hydrogen-bonding structure like that of liquid water. The
95 NEXAFS spectrum of sodium chloride – ice mixtures (Fig. 1E) at 249 K are indistinguishable from those of hydrohalite. Taken
96 the spectra quality and the small difference in the shape of the liquid and of the hydrohalite spectrum, it is beyond the scope
97 of this work to elaborate whether the NEXAFS spectrum in Fig. 1E might be understood by deconvoluting it in its hydrohalite
98 and brine components and by this reveal a fraction of the chloride being embedded in a brine-like hydrogen bonding network.

99 Krepelova et al. (2010a)'s oxygen K-edge spectra of sodium chloride -- ice did not reveal water molecules being coordinated
100 like in the liquid. Taken together it seems likely that the chloride at the hydrohalite – air interface does not engage in forming
101 solvation shells similar to those in aqueous solutions and that the signal from the hydrohalite by far exceeds the signal from a
102 chloride that might migrate to the ice surfaces in intensity.

103 **Nucleation in absence of ice**

104 Hydrohalite can also precipitate in absence of ice by evaporating water from a solution at temperatures below 273 K (Craig et
105 al., 1975; Yang et al., 2017). Such a trajectory, that is the temperature and water vapor pressure the sample experienced, is
106 shown in Fig. 2C (green solid line). At 244 K and 59 % RH, in absence of ice, nucleation was visually observed and a NEXAFS
107 spectrum was recorded that was identified as hydrohalite. The location in the phase diagram is in agreement with Wagner et
108 al. (2012)'s observation of salt deposits in aerosol droplets in the AIDA chamber in absence of ice. The sample at 44 % RH
109 (Fig 2C, blue line) has been exposed to 0 % RH prior to acquiring the NEXAFS spectrum, which removes the crystal water
110 (Light et al., 2009; Wise et al., 2012). The NEXAFS spectrum recorded at 248 K and 44 % RH (Fig 1A) shows that no
111 deliquescence occurred and thus serves as reference for a halite spectrum. We note that we misinterpreted this spectrum as that
112 of hydrohalite in our previous technical paper introducing the NAPP end station (Orlando et al., 2016).

113
114 The halite spectrum (Fig. 1A, Fig. 2C blue square) was recorded at 44 % RH, a humidity where water readily adsorbs on
115 surfaces (Blum, 2010), and the presence of water at the sodium chloride - air interface at elevated RH has been demonstrated
116 previously (Ewing, 2005; Wise et al., 2008). A further reason for the presence of water at lower RH than the deliquescence
117 might be sodium chloride's high solubility. Kong et al. (2020) has recently suggested that sodium ions from sodium acetate
118 are dissolved in adsorbed water prior to deliquescence. Indications for solvation of halide ions on single crystals below
119 deliquescence relative humidity were also reported previously (Luna et al., 1998). An analogue investigation was beyond the
120 scope of this work. The fact that we find no indication for a dominant liquid feature in the upper 6 nm of the sodium chloride
121 – air interface based on the chlorine X-ray absorption spectrum might be due to probing deeper into the interfacial region in
122 this work as compared to Kong et al. (2020).

123 **NaCl or NaCl.2H2O**

124 We have shown that in presence of ice, hydrohalite precipitates; halite was not observed in this study except when crystal
125 water was removed in vacuum. This is in agreement with Koop et al. (2000) who found precipitation of hydrohalite in presence
126 of ice and suggested that heterogenous nucleation at ice surfaces favours nucleation of hydrohalite. Studies with liquid droplets
127 in absence of ice found both halite and hydrohalite precipitating in the thermodynamic stability domain of the hydrohalite
128 (Wagner et al., 2011; Wise et al., 2012; Peckhaus et al., 2016). The transition between crystallization of halite and hydrohalite
129 at between 253 K to 241 K was explained based on nucleation theory and the deviating trend of nucleation rate of both species
130 with temperature (Peckhaus et al., 2016). That hydrohalite crystallizes in absence of ice in our study shows that also gold

31 surfaces, of the sample holder, serve as good nucleation support for hydrohalite. It appears that any specific properties of the
32 ice surface, as compared to gold, are of minor importance. In agreement, Wagner et al. (2015) showed efficient nucleation of
33 hydrohalite in droplets containing solid oxalic acid and halite precipitated in absence of oxalic acid at the same temperature
34 and relative humidity.

35 **1 Summary and Atmospheric Implication**

36 The upper 6 nm of the interfacial region of a sodium chloride – ice binary system was investigated in this study at various
37 positions in the phase diagram. The sample was always in equilibrium with gas-phase water which makes cooling conditions
38 and concentrations of the brine identical to aerosol particles embedded in snow or in the troposphere. The inherent sensitivity
39 to the interfacial region comes from using partial Auger-Meitner electron yield NEXAFS and the limited pathlength of
40 electrons travelling in matter. With a probing depth of a few nanometre, the interfacial region is probed spanning from the
41 upper molecular layers somewhat into the bulk (Ammann et al., 2018). In this work, we describe the NEXAFS spectrum of
42 hydrohalite for the first time.

43
44 The results emphasise that the nucleation of hydrohalite is a function of both the temperature and the relative humidity. While
45 we show that the nucleation of hydrohalite at the interface is favoured by surfaces, we find supercooled solution of sodium
46 chloride in the interfacial region of ice. The supercooled solutions have been observed to be metastable for hours in these
47 experiments. This has direct implications for heterogeneous chemistry in cold parts of Earth's environment. Multiphase
48 reactions may proceed at accelerated rates in these highly concentrated brines at temperatures ~10 degrees below the eutectic
49 compared to reactions on solid hydrohalite. In this respect, there is no difference in the interfacial region to liquid embedded
50 in the bulk of snow and ice samples. This implies that when chemical reactivity of ice and snow is discussed, knowledge of its
51 thermal history is essential. From temperature and relative humidity alone, nucleation or efflorescence cannot be predicted at
52 the interface as in the bulk.

53
54 We suggest that the brine observed by Cho et al. (2002) is a consequence of micro-pockets. Because these are only observed
55 at low concentration of the solution before freezing of ice, but aerosol at typical relative humidity that prevail in cold parts of
56 the atmosphere are highly concentrated, we suggest that micro-pockets in the interfacial region small enough to establish a
57 significant depression in freezing point at the air-ice interface are of small relevance to the environment.

58

59 **Data Availability**

60 Bartels-Rausch, Thorsten (2020). Data set on interfacial supercooling and the precipitation of hydrohalite in frozen NaCl
61 solutions by X-ray absorption spectroscopy. EnviDat. [doi:10.16904/enviDat.164](https://doi.org/10.16904/enviDat.164).

62 **Acknowledgement**

63 Funding by the Swiss National Science Foundation (SNSF) under Grant No. 149629 is acknowledged. We thank Mario Birrer
64 (PSI) for his technical assistance. TB-R thanks Peter Alpert for stimulating discussion in our office.

65 **Author Contribution**

66 TB-R designed and planned the study, analysed the data, and wrote the manuscript. FO, LA, MA, TH planned and optimised
67 beamline and electron analyser settings. XK, AW, LA, and TBR performed the experiments. All authors approved the
68 submitted version of the manuscript.

70 **References**

- 71
72 Abbatt, J. P. D., Thomas, J. L., Abrahamsson, K., Boxe, C. S., Granfors, A., Jones, A. E., King, M. D., Saiz-Lopez, A.,
73 Shepson, P. B., Sodeau, J. R., Toohey, D. W., Toubin, C., von Glasow, R., Wren, S. N., and Yang, X.: Halogen activation via
74 interactions with environmental ice and snow in the polar lower troposphere and other regions, *Atmos. Chem. Phys.*, 12, 6237-
75 6271, 10.5194/acp-12-6237-2012, 2012.
- 76 Ammann, M., Artiglia, L., and Bartels-Rausch, T.: X-ray excited electron spectroscopy to study gas-liquid interfaces of
77 atmospheric relevance, in: *Physical chemistry of gas-liquid interfaces*, Elsevier, 135-166, 2018.
- 78 Antalek, M., Pace, E., Hedman, B., Hodgson, K. O., Chillemi, G., Benfatto, M., Sarangi, R., and Frank, P.: Solvation structure
79 of the halides from x-ray absorption spectroscopy, *J. Chem. Phys.*, 145, 044318, 10.1063/1.4959589, 2016.
- 80 Aristov, Y. I., Di Marco, G., Tokarev, M. M., and Parmon, V. N.: Selective water sorbents for multiple applications, 3. CaCl₂
81 solution confined in micro- and mesoporous silica gels: Pore size effect on the “solidification-melting” diagram, *React. Kinet.*
82 *Catal. Lett.*, 61, 147-154, 10.1007/BF02477527, 1997.
- 83 Artiglia, L., Edebeli, J., Orlando, F., Chen, S., Lee, M.-T., Corral Arroyo, P., Gilgen, A., Bartels-Rausch, T., Kleibert, A.,
84 Vazdar, M., Carignano, M. A., Francisco, J. S., Shepson, P. B., Gladich, I., and Ammann, M.: A surface-stabilized ozonide
85 triggers bromide oxidation at the aqueous solution-vapour interface, *Nat. Commun.*, 8, 700, 10.1038/s41467-017-00823-x,
86 2017.
- 87 Bartels-Rausch, T., Jacobi, H.-W., Kahan, T. F., Thomas, J. L., Thomson, E. S., Abbatt, J. P. D., Ammann, M., Blackford, J.
88 R., Bluhm, H., Boxe, C. S., Dominé, F., Frey, M. M., Gladich, I., Guzman, M. I., Heger, D., Huthwelker, T., Klan, P., Kuhs,
89 W. F., Kuo, M. H., Maus, S., Moussa, S. G., McNeill, V. F., Newberg, J. T., Pettersson, J. B. C., Roeselova, M., and Sodeau,
90 J. R.: A review of air-ice chemical and physical interactions (AICI): Liquids, quasi-liquids, and solids in snow, *Atmos. Chem.*
91 *Phys.*, 14, 1587-1633, 10.5194/acp-14-1587-2014, 2014.
- 92 Bartels-Rausch, T., Orlando, F., Kong, X., Artiglia, L., and Ammann, M.: Experimental evidence for the formation of solvation
93 shells by soluble species at a nonuniform air-ice interface, *ACS Earth Space Chem.*, 1, 572-579,
94 10.1021/acsearthspacechem.7b00077, 2017.

95 Blackford, J. R.: Sintering and microstructure of ice: A review, *J. Phys. D: Appl. Phys.*, 40, R355-R385, 10.1088/0022-
96 3727/40/21/R02, 2007.

97 Blackford, J. R., Jeffree, C. E., Noake, D. F. J., and Marmo, B. A.: Microstructural evolution in sintered ice particles containing
98 NaCl observed by low-temperature scanning electron microscope, *Proc. Inst. Mech. Eng.*, 221, 151-156,
99 10.1243/14644207JMDA134, 2007.

00 Bluhm, H., Ogletree, D. F., Fadley, C. S., Hussain, Z., and Salmeron, N.: The premelting of ice studied with photoelectron
01 spectroscopy, *J. Phys.: Condens. Matter*, 14, L227-L233, 10.1088/0953-8984/14/8/108, 2002.

02 Bluhm, H.: Photoelectron spectroscopy of surfaces under humid conditions, *Journal of Electron Spectroscopy and Related
03 Phenomena*, 177, 71-84, 10.1016/j.elspec.2009.08.006, 2010.

04 Cho, H., Shepson, P. B., Barrie, L. A., Cowin, J. P., and Zaveri, R.: NMR investigation of the quasi-brine layer in ice/brine
05 mixtures, *J. Phys. Chem. B*, 106, 11226-11232, 10.1021/jp020449+, 2002.

06 Christenson, H. K.: Confinement effects on freezing and melting, *J. Phys.: Condens. Matter*, 13, R95-R133, 10.1088/0953-
07 8984/13/11/201, 2001.

08 Cleff, B., and Mehlhorn, W.: Das KLL- Auger-Spektrum von Chlor, *Z. Phys. A: Hadrons Nucl.*, 219, 311-324,
09 10.1007/BF01395528, 1969.

10 Craig, J. R., Light, J. F., Parker, B. C., and Mudrey, M. G.: Identification of hydrohalite, *Antarctic Journal of the United States*,
11 10, 178-179, 1975.

12 Evans, K. A., Mavrogenes, J. A., O'Neill, H. S., Keller, N. S., and Jang, L. Y.: A preliminary investigation of chlorine XANES
13 in silicate glasses, *Geochim. Geophys. Geosyst.*, 9, 10.1029/2008gc002157, 2008.

14 Ewing, G. E.: H₂O on NaCl: From single molecule, to clusters, to monolayer, to thin film, to deliquescence, in, *Chapter 12*,
15 Springer-Verlag, Berlin/Heidelberg, 1-25, 2005.

16 Finlayson-Pitts, B. J.: The tropospheric chemistry of sea salt: A molecular-level view of the chemistry of NaCl and NaBr,
17 *Chem. Rev.*, 103, 4801-4822, 10.1021/cr020653t, 2003.

18 Fujimori, T., Takaoka, M., and Morisawa, S.: Chlorinated aromatic compounds in a thermal process promoted by
19 oxychlorination of ferric chloride, *Environ. Sci. Technol.*, 44, 1974-1979, 10.1021/es903337d, 2010.

20 Gladich, I., Chen, S., Vazdar, M., Boucly, A., Yang, H., Ammann, M., and Artiglia, L.: Surface propensity of aqueous
21 atmospheric bromine at the liquid-gas interface, *J Phys Chem Lett*, 11, 3422-3429, 10.1021/acs.jpcclett.0c00633, 2020.

22 Grannas, A. M., Bausch, A. R., and Mahanna, K. M.: Enhanced aqueous photochemical reaction rates after freezing, *J. Phys.
23 Chem. A*, 111, 11043-11049, 10.1021/jp073802q, 2007.

24 Harada, M., Tasaki, Y., Tasaki, Y., Qu, H., and Okada, T.: Hydration of ions and salt crystallization in liquid phase coexistent
25 with ice at temperature below eutectic point, *RSC Advances*, 2, 461-466, 10.1039/c1ra00801c, 2011.

26 Huggins, F. E., and Huffman, G. P.: Chlorine in coal - an XAFS spectroscopic investigation, *Fuel*, 74, 556-569, 10.1016/0016-
27 2361(95)98359-m, 1995.

28 Hullar, T., and Anastasio, C.: Direct visualization of solute locations in laboratory ice samples, *Cryosphere*, 10, 2057-2068,
29 10.5194/tc-10-2057-2016, 2016.

30 Kahan, T. F., Wren, S. N., and Donaldson, D. J.: A pinch of salt is all it takes: Chemistry at the frozen water surface, *Acc.
31 Chem. Res.*, 47, 1587-1594, 10.1021/ar5000715, 2014.

32 Klewe, B., Pedersen, B., and Iucr: The crystal structure of sodium chloride dihydrate, *Acta Crystallogr., Sect. B*, 30, 2363-
33 2371, 10.1107/S0567740874007138, 1974.

34 Knipping, E. M., Lakin, M. J., Foster, K. L., Jungwirth, P., Tobias, D. J., Gerber, R. B., Dabdub, D., and Finlayson-Pitts, B.
35 J.: Experiments and simulations of ion-enhanced interfacial chemistry on aqueous NaCl aerosols, *Science*, 288, 301-306,
36 10.1126/science.288.5464.301, 2000.

37 Kong, X., Waldner, A., Orlando, F., Artiglia, L., Huthwelker, T., Ammann, M., and Bartels-Rausch, T.: Coexistence of
38 physisorbed and solvated HCl at warm ice surfaces, *J. Phys. Chem. Lett.*, 8, 4757-4762, 10.1021/acs.jpcclett.7b01573, 2017.

39 Kong, X., Castarède, D., Boucly, A., Artiglia, L., Ammann, M., Bartels-Rausch, T., Thomson, E. S., and Pettersson, J. B. C.:
40 Reversibly physisorbed and chemisorbed water on carboxylic salt surfaces under atmospheric conditions, *J. Phys. Chem. C*,
41 124, 5263-5269, 10.1021/acs.jpcc.0c00319, 2020.

42 Koop, T., Kapilashrami, A., Molina, L. T., and Molina, M. J.: Phase transitions of sea-salt/water mixtures at low temperatures:
43 Implications for ozone chemistry in the polar marine boundary layer, *J. Geophys. Res.*, 105, 26393-26402,
44 10.1029/2000JD900413, 2000.

45 Krepelova, A., Huthwelker, T., Bluhm, H., and Ammann, M.: Surface chemical properties of eutectic and frozen NaCl
46 solutions probed by XPS and NEXAFS, *Chem. Phys. Chem.*, 11, 3859-3866, 10.1002/cphc.201000461, 2010a.
47 Krepelova, A., Newberg, J. T., Huthwelker, T., Bluhm, H., and Ammann, M.: The nature of nitrate at the ice surface studied
48 by XPS and NEXAFS, *Phys. Chem. Chem. Phys.*, 12, 8870-8880, 10.1039/c0cp00359j, 2010b.
49 Krepelova, A., Bartels-Rausch, T., Brown, M. A., Bluhm, H., and Ammann, M.: Adsorption of acetic acid on ice studied by
50 ambient-pressure XPS and partial-electron-yield NEXAFS spectroscopy at 230–240 K, *J. Phys. Chem. A*, 117, 401-409,
51 10.1021/jp3102332, 2013.
52 Laskin, A., Wang, H., Robertson, W. H., Cowin, J. P., Ezell, M. J., and Finlayson-Pitts, B. J.: A new approach to determining
53 gas-particle reaction probabilities and application to the heterogeneous reaction of deliquesced sodium chloride particles with
54 gas-phase hydroxyl radicals, *J. Phys. Chem. A*, 110, 10619-10627, 10.1021/jp063263+, 2006.
55 Light, B., Brandt, R. E., and Warren, S. G.: Hydrohalite in cold sea ice: Laboratory observations of single crystals, surface
56 accumulations, and migration rates under a temperature gradient, with application to “snowball earth”, *J. Geophys. Res.*, 114,
57 C07018, 10.1029/2008JC005211, 2009.
58 Luna, M., Rieutord, F., Melman, N. A., Dai, Q., and Salmeron, M.: Adsorption of water on alkali halide surfaces studied by
59 scanning polarization force microscopy, *J. Phys. Chem. A*, 102, 6793-6800, 10.1021/jp9820875, 1998.
60 Malley, P. P. A., Chakraborty, S., and Kahan, T. F.: Physical characterization of frozen saltwater solutions using Raman
61 microscopy, *ACS Earth Space Chem.*, 2, 702-710, 10.1021/acsearthspacechem.8b00045, 2018.
62 Marti, J., and Mauersberger, K.: A survey and new measurements of ice vapor pressure at temperatures between 170 and 250
63 K, *Geophys. Res. Lett.*, 20, 363-366, 10.1029/93GL00105, 1993.
64 Maus, S., Huthwelker, T., Enzmann, F., Miedaner, M. M., Stampanoni, M., Marone, F., Hutterli, M. A., Hintermüller, C.,
65 Hintermüller, C., and Kersten, M.: Synchrotron-based X-ray micro-tomography: Insights into sea ice microstructure, Sixth
66 Workshop on Baltic Sea Ice Climate, Lammi Biological Station, Finland, Aug 25, 2008.
67 Maus, S., Huthwelker, T., Schwikowski, M., and Enzmann, F.: Ion fractionation in young sea ice from Kongsfjorden, svalbard,
68 *Annals of Glaciology*, 52, 301-310, Doi 10.3189/172756411795931804, 2011.
69 Newberg, J. T., and Bluhm, H.: Adsorption of 2-propanol on ice probed by ambient pressure X-ray photoelectron spectroscopy,
70 *Phys. Chem. Chem. Phys.*, 17, 23554-23558, 10.1039/C5CP03821A, 2015.
71 Nilsson, A., Nordlund, D., Waluyo, I., Huang, N., Ogasawara, H., Kaya, S., Bergmann, U., Näslund, L. A., Öström, H., Wernet,
72 P., Andersson, K. J., Schiros, T., and Pettersson, L. G. M.: X-ray absorption spectroscopy and X-ray Raman scattering of water
73 and ice; an experimental view, *Journal of Electron Spectroscopy and Related Phenomena*, 177, 99-129,
74 10.1016/j.elspec.2010.02.005, 2010.
75 Nye, J. F.: Thermal behaviour of glacier and laboratory ice, *J. Glaciol.*, 37, 401-413, 10.3189/S0022143000005839, 1991.
76 Obbard, R. W., Troderman, G., and Baker, I.: Imaging brine and air inclusions in sea ice using micro-X-ray computed
77 tomography, *J. Glaciol.*, 55, 1113-1115, Doi 10.3189/002214309790794814, 2009.
78 Oldridge, N. W., and Abbatt, J. P. D.: Formation of gas-phase bromine from interaction of ozone with frozen and liquid
79 NaCl/NaBr solutions: Quantitative separation of surficial chemistry from bulk-phase reaction, *J. Phys. Chem. A*, 115, 2590-
80 2598, 10.1021/jp200074u, 2011.
81 Orlando, F., Waldner, A., Bartels-Rausch, T., Birrer, M., Kato, S., Lee, M.-T., Proff, C., Huthwelker, T., Kleibert, A., van
82 Bokhoven, J. A., and Ammann, M.: The environmental photochemistry of oxide surfaces and the nature of frozen salt solutions:
83 A new in situ XPS approach, *Top. Catal.*, 59, 591-604, 10.1007/s11244-015-0515-5, 2016.
84 Osthoff, H. D., Roberts, J. M., Ravishankara, A. R., Williams, E. J., Lerner, B. M., Sommariva, R., Bates, T. S., Coffman, D.,
85 Quinn, P. K., Dibb, J. E., Stark, H., Burkholder, J. B., Talukdar, R. K., Meagher, J., Fehsenfeld, F. C., and Brown, S. S.: High
86 levels of nitryl chloride in the polluted subtropical marine boundary layer, *Nat. Geosci.*, 1, 324-328, 10.1038/ngeo177, 2008.
87 Peckhaus, A., Kiselev, A., Wagner, R., Duft, D., and Leisner, T.: Temperature-dependent formation of NaCl dihydrate in
88 levitated NaCl and sea salt aerosol particles, *J. Chem. Phys.*, 145, 244503, 10.1063/1.4972589, 2016.
89 Saiz-Lopez, A., and von Glasow, R.: Reactive halogen chemistry in the troposphere, *Chem. Soc. Rev.*, 41, 6448-6472,
90 10.1039/C2CS35208G, 2012.
91 Rumble, J., *CRC handbook of chemistry and physics*, 100th edition, CRC Press/Taylor & Francis, Boca Raton, FL., 2019.
92 Simpson, W. R., von Glasow, R., Riedel, K., Anderson, P., Ariya, P., Bottenheim, J., Burrows, J., Carpenter, L. J., Friess, U.,
93 Goodsite, M. E., Heard, D., Hutterli, M., Jacobi, H. W., Kaleschke, L., Neff, B., Plane, J., Platt, U., Richter, A., Roscoe, H.,

94 Sander, R., Shepson, P., Sodeau, J., Steffen, A., Wagner, T., and Wolff, E.: Halogens and their role in polar boundary-layer
95 ozone depletion, *Atmos. Chem. Phys.*, 7, 4375-4418, 10.5194/acp-7-4375-2007, 2007.

96 Simpson, W. R., Brown, S. S., Saiz-Lopez, A., Thornton, J. A., and von Glasow, R.: Tropospheric halogen chemistry: Sources,
97 cycling, and impacts, *Chem. Rev.*, 115, 4035-4062, 10.1021/cr5006638, 2015.

98 Tanuma, S., Powell, C. J., and Penn, D. R.: Calculations of electron inelastic mean free paths: 3. Data for 15 inorganic-
99 compounds over the 50-2000 eV range, *Surf. Interface Anal.*, 17, 927-939, 10.1002/sia.740171305, 1991.

00 Tasaki, Y., Harada, M., and Okada, T.: Eutectic transition of local structure for bromide ion in bulk and on surface of doped
01 ice, *J. Phys. Chem. C*, 114, 12573-12579, 10.1021/jp102246f, 2010.

02 Thornton, J. A., Kercher, J. P., Riedel, T. P., Wagner, N. L., Cozic, J., Holloway, J. S., Dube, W. P., Wolfe, G. M., Quinn, P.
03 K., Middlebrook, A. M., Alexander, B., and Brown, S. S.: A large atomic chlorine source inferred from mid-continental
04 reactive nitrogen chemistry, *Nature*, 464, 271-274, 10.1038/nature08905, 2010.

05 Wagner, R., Möhler, O., Saathoff, H., Schnaiter, M., and Leisner, T.: New cloud chamber experiments on the heterogeneous
06 ice nucleation ability of oxalic acid in the immersion mode, *Atmos. Chem. Phys.*, 11, 2083-2110, 10.5194/acp-11-2083-2011,
07 2011.

08 Wagner, R., Mohler, O., and Schnaiter, M.: Infrared optical constants of crystalline sodium chloride dihydrate: Application to
09 study the crystallization of aqueous sodium chloride solution droplets at low temperatures, *J Phys Chem A*, 116, 8557-8571,
10 10.1021/jp306240s, 2012.

11 Wagner, R., Höhler, K., Möhler, O., Saathoff, H., and Schnaiter, M.: Crystallization and immersion freezing ability of oxalic
12 and succinic acid in multicomponent aqueous organic aerosol particles, *Geophys. Res. Lett.*, 42, 2464-2472,
13 10.1002/2015GL063075, 2015.

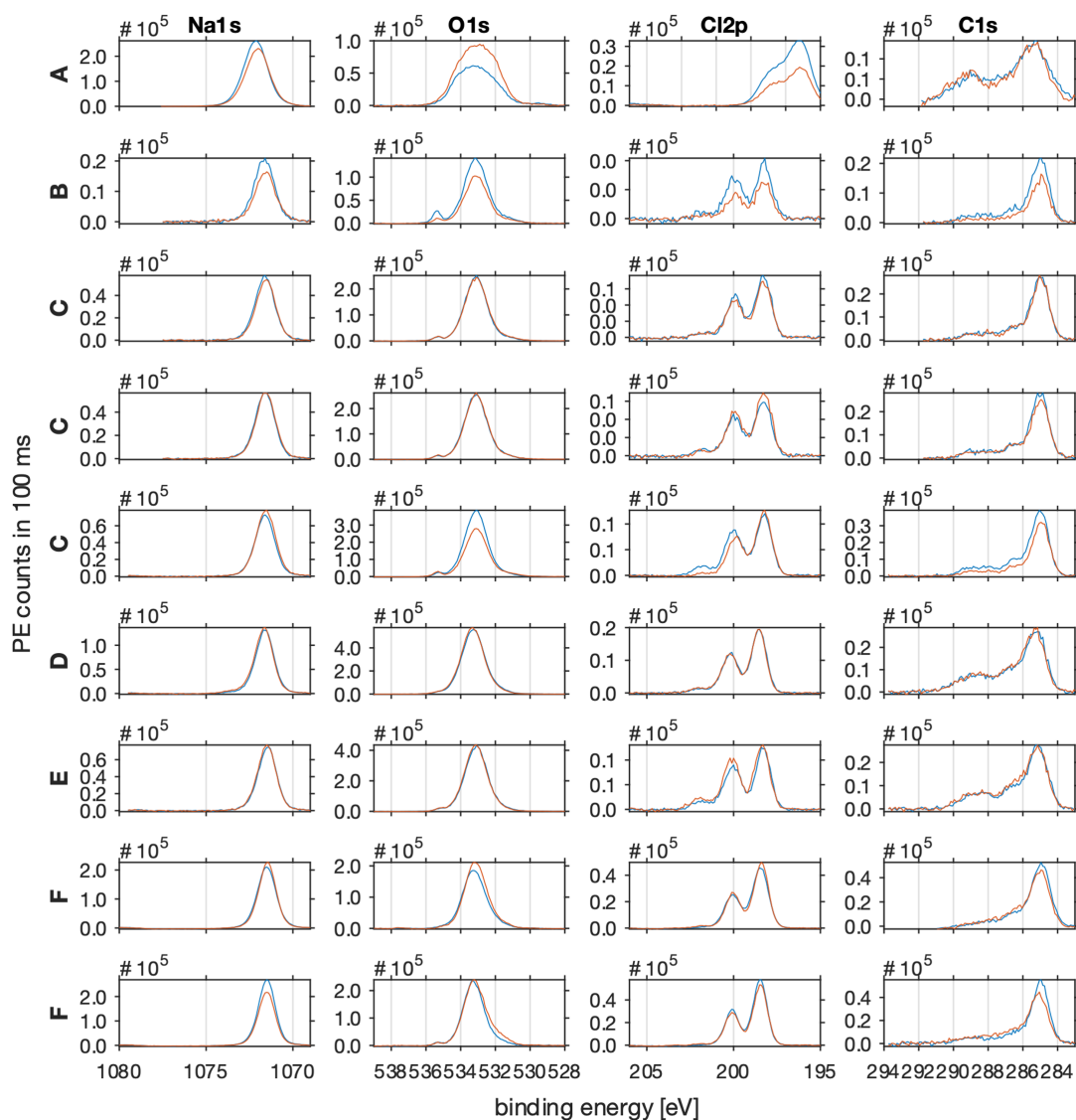
14 Waldner, A., Artiglia, L., Kong, X., Orlando, F., Huthwelker, T., Ammann, M., and Bartels-Rausch, T.: Pre-melting and the
15 adsorption of formic acid at the air-ice interface at 253 K as seen by NEXAFS and XPS, *Phys. Chem. Chem. Phys.*, 20, 24408-
16 24417, 10.1039/C8CP03621G, 2018.

17 Wise, M. E., Martin, S. T., Russell, L. M., and Buseck, P. R.: Water uptake by NaCl particles prior to deliquescence and the
18 phase rule, *Aerosol Sci. Technol.*, 42, 281-294, 10.1080/02786820802047115, 2008.

19 Wise, M. E., Baustian, K. J., Koop, T., Freedman, M. A., Jensen, E. J., and Tolbert, M. A.: Depositional ice nucleation onto
20 crystalline hydrated NaCl particles: A new mechanism for ice formation in the troposphere, *Atmos. Chem. Phys.*, 12, 1121-
21 1134, 10.5194/acp-12-1121-2012, 2012.

22 Yang, X., Neděla, V., Runštuk, J., Ondrušková, G., Krausko, J., Vetráková, L., and Heger, D.: Evaporating brine from frost
23 flowers with electron microscopy and implications for atmospheric chemistry and sea-salt aerosol formation, *Atmos. Chem.*
24 *Phys.*, 17, 6291-6303, 10.5194/acp-17-6291-2017, 2017.

25
26



28

29 This Figure shows the photo emission intensities as acquired before (blue line) and after (red line) each NEXAFS spectrum.

30 The PE spectra of sodium (Na1s) are shown in column 1, of oxygen (O1s) in column 2, of chlorine (Cl2p) in column 3, and of
31 carbon (C1s) in column 4. All spectra were acquired at the Phoenix beam line of SLS of PSI with a photon energy of 2200 eV.32 Pass energy was set to 100 eV and dwell time to 100 ms. Beam line slits were 2 x 2 mm. The C-H feature at 285 eV of the C1s
33 photoemission spectra served as binding energy reference and all spectra were shifted by 4-5.5 eV to account for charging

34 effects.

35

36 The spectra can be described as follows:

- 37 • The Na1s region shows one gauss-shaped feature at 1072 eV as expected for sodium.
- 38 • The O1s region shows one dominant feature at 535 eV in line with oxygen in ice and a smaller feature at higher
39 binding energy which might be attributed to gas-phase water.
- 40 • The Cl2p region shows the typical doublet of the p-orbital spin-orbit splitting (p(3/2) and p(1/2)), 1.6 eV apart at 200
41 eV binding energy. Additionally, in some spectra a small feature at 203 eV binding energy is evident which might
42 be attributed to the Cl2p(1/2) of organic carbon species.
- 43 • The C1s region shows a broad spectrum with the main feature at 285 eV binding energy, typical for the C-H of
44 adventitious carbon. The overlapping features at higher binding energy can be attributed to C-OH, C=O, C(O)=O and
45 C-Cl.
- 46 • The spectra of all species acquired before and after the sample in Figure A are significantly wider compared to the
47 other samples. Additionally, the Cl2p features are shifted by 2 eV to lower binding energy. This sample is, unlike the
48 others, is characterised by a large variation in sample thickness (Figure 3A of manuscript) which leads to differential
49 charging and might explain the wider peak shapes and shift in the Cl2p features.
- 50 • In sample A, the photoemission intensities of the Na1s and Cl2p show a higher intensity after the NEXAFS spectrum
51 was acquired compared to before. During that time, the photoemission intensity of O1s increased. This suggests that
52 water kept adsorbing to the sample and masked the signal intensity of the underlying sodium chloride.
- 53 • In sample B, all photoemission intensities decreased during the time it took to acquire the NEXAFS spectra. This
54 suggests that the working distances changed which impacts the sensitivity of all sample components.

55

56

57

58

59